24th COBEM - 2017

24th ABCM International Congress of Mechanical Engineering
December 3-8, 2017, Curitiba, PR, Brazil

COBEM-2017-2116
SIMULATION AND EXPERIMENTAL VALIDATION OF THE DYNAMIC MODELING OF A 3-RPR MECHANISM USING POWER FLOW APPROACH

Albuquerque, A. N.
Speranza Neto, M.
Meggiolaro, M. A.
Pontifical Catholic University of Rio de Janeiro, Department of Mechanical Engineering, Rio de Janeiro, Brazil
allan@puc-rio.br, msn@puc-rio.br, meggi@puc-rio.br

Abstract. *Mechanisms are essentially made up of multiple rigid bodies that have relative motion between themselves. Each body is connected through a joint to one or more bodies, wherein the sequence of connected bodies is called kinematic chain. Open kinematic chains have no restrictions on their ends, as closed chains have restrictions on both ends. The focus in this work will be given on the study of mechanisms with closed kinematic chains. Thus, this work presents the analytical form determination of the dynamic model of a parallel planar mechanism with three degrees of freedom through the characterization of the power flow between its components. Considering the power flow between the degrees of freedom, and also between these and the actuating elements (linear electric actuators) the equilibrium relations of the forces and torques are obtained. Accounting for inertial effects of system components, the stiffness and damping effects, the equations of motion are analytically determined. Besides, the relation between the inverse kinematics and the direct dynamics is presented. The proposed methodology is generalized and applicable in any type of mechanism. A set of simulations are performed to validate this approach using the real data from a planar mechanism designed and built especially for the purpose to compare the simulated and experimental results. This comparison validates the dynamic model and the analytical equations lead to a more efficient simulation process and real-time control of these systems. Finally, a closed-loop control strategy using the inverse kinematic and the direct dynamic models is proposed.*

Keywords: *Parallel Mechanisms, Inverse Kinematics, Direct Dynamics, Power Flow, Bond Graphs*

1. INTRODUCTION

Mechanisms are essentially (but not exclusively) made up of multiple rigid bodies that have relative motion between themselves. Each rigid body is connected through a joint to one or more bodies, wherein the serial sequence of connected bodies is called kinematic chain. Open kinematic chains have no restrictions on their ends, as closed chains have restrictions on both ends. In this work, the focus will be given on the study of mechanisms with closed kinematic chains. Despite of having a smaller workspace, higher inertia and a harder dynamic analysis, parallel systems have great advantages when compared to serial manipulators, as better stability and accuracy, ability to handle relatively large loads, high velocities and accelerations and low power operation (Wang, 2008).

1.1 Parallel mechanisms

The improvement in the modeling of parallel mechanisms also contributes to solve problems associated with some serial robots tasks. In some tasks, such as when a serial robotic arm opens a door or engages its end effector to a surface or object, the kinematic chain, due to the appearance of restrictions in the degrees of freedom of the end effector, is temporarily closed (Bennett *et al.*, 1991). Another case in which a serial mechanism becomes a closed kinematic chain is the case of the legs of an anthropomorphic robot. When both feet found a restriction (such as the floor, for example), the kinematic chain closes and thus, to estimate the robot's hip movement in order to balance it, multi-branch mechanisms or parallel mechanisms modeling techniques are used (Khandelwal *et al.*, 2013).

Mohamed *et al*. (2005) deals with the kinematics of parallel mechanisms with several closed chains separating the Jacobian matrices of mechanism’s active and passive joints. Kim *et al*. (2001) proposed a two-step solution process: cutting operation and paste operation, that is, a restriction is removed and the model works as the kinematic chain was opened, and then a solution that meets the original closed chain is found. In Fischer *et al*. (2001) the Denavit-Hartenberg and Sheth-Uicker notations were used for kinematic modeling of various types of parallel mechanisms, such as the Whitworth quick return mechanism. In Goulin *et al*. (2011) the static modeling of a 3-RPR parallel robot is made by using the graphs theory in the problem of topological modeling and in the derivation of the equations of balance, where the mechanical quantities (movements and actions) are described by helicoids (Davies method).

1.2 Power flow approach

Created by H. M. Paynter in the late 50's and developed by D. C. Karnopp and R. C. Rosenberg (Karnopp *et al*., 1968; Rosenberg *et al*., 1983 and Karnopp *et al*., 1990) in the mid-60's, the bond graphs technique are characterized by the physical model representation of a system through a logical graphic, where the energy flow and the system components information are contained (Speranza Neto *et al*., 2005).

In Costa Neto (2008) the mathematical models of subsystems using power flow were created so that it was possible to implement them as separate and interchangeable modules in a block diagram, coupling them directly, in computational form. The independent modules are tested individually, being possible to separate kinematics and dynamics. The method used to open the algebraic loops of the closed chain mechanisms eliminates the algebraic equations that characterize the loop. Once the module is created, no adjustment needs to be made in the overall structure of the system.

Zhao *et al*. (2012) used the same technique to model the kinematics and dynamics of a Stewart platform. After the kinematic modeling, the dynamic equations of the upper platform were developed using the Newton-Euler method and then, its model in bond graph has been established. An equivalent approach is used to handle the inertial effects of each actuator. In each actuator-valve set of the simulator an independent position closed loop control is coupled. The bond graph model is made using the software *20-sim* and then, several simulations are realized to verify the model. A comparison with experimental tests proved the feasibility and efficiency of the model, whose the method can be used to model other types of parallel mechanisms.

In his work, Yildiz *et al.* (2008) represented the Stewart platform dynamics using a novel spatial visualization form of the bond graphs. This dynamic model includes all the dynamic and gravitational effects such as the linear motor dynamics (used as an actuator) and the viscous friction of the joints. Furthermore, in this work the actuation system and the structure modeling are unified. As this system has many nonlinearities, originated by your non-linear geometry and the gyroscopic forces, the problem of the resulting derivative (forced) causality due to the rigidly coupled inertial elements is approached and the space-state equations are presented.

1.3 Procedure

The proposed methodology is generalized and applicable in any type of mechanism (open or closed, planar or spatial). For a better comprehension of the methodology, a planar case will be discussed in this work. The inverse kinematic model of the closed chain mechanism, which has easy solution when compared to the direct model, can be developed by any known methodology, without the need for a systematic approach. It begins by determining the inverse geometric model and its derivation to obtain the kinematic relations, and therefore the inverse Jacobian matrix. With the inverse kinematic model, the inverse kinematics bond graph is built and, from the cause and effect relations, the direct dynamic model of the mechanism is found. Thus, this methodology (bond graphs or power flow) is more efficient and secure to achieve the dynamic analytical (closed) models of parallel mechanisms. For the purpose of provide real data (geometry, inertia, damping, actuators forces, etc.) and compare the simulated and experimental results, a planar mechanism was designed and built. Figure 1 shows the built platform.

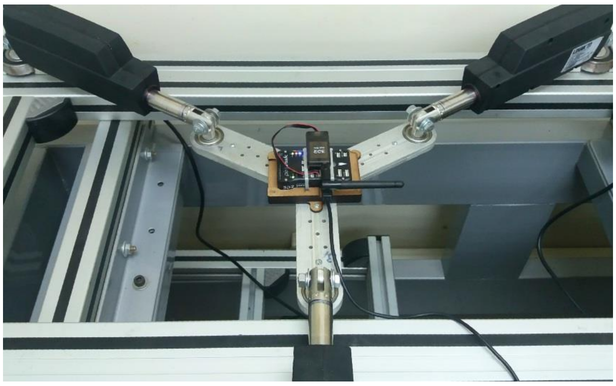

Figure 1. The built planar mechanism.

2. DYNAMIC MODEL USING POWER FLOW APPROACH

2.1 Inverse kinematic model

Figure 2 shows the 3-RPR parallel manipulator considered in this study. Three limbs connects to the mobile platform and the fixed base by rotational joints in points B_i and A_i, i = 1, 2 e 3. To describe its geometry, a referential frame A(X, Y) fixed to the platform base is added and other frame, B(x, y), is coupled to the mobile platform. Another reference frame, C(x_i, y_i), is fixed to each rotational joint, thus having its origin at the point A_i (i = 1, 2 e 3). The y_i axis of this system points from A_i to B_i (direction of the actuator i). For convenience, the origin of the frame B is located at the center of the mobile platform. The position of the mobile platform can be described by the vector $\boldsymbol{p} = [p_X, p_Y]^T = [X, Y]^T$ and by the rotation matrix ${}^{A}\mathbf{R}_{B}$. Hence, the velocities state of the mobile platform is defined as a three dimensional vector with the absolute linear velocity and the angular velocity of the mobile platform (Eq. 1).

$$\dot{\mathbf{x}} = \mathbf{v} = \begin{bmatrix} \mathbf{v}_p \\ \boldsymbol{\omega}_p \end{bmatrix} = \begin{bmatrix} \dot{X} \\ \dot{Y} \\ \dot{\theta} \end{bmatrix} = \begin{bmatrix} v_X \\ v_Y \\ \omega_z \end{bmatrix} \tag{1}$$

For this manipulator, the input vector is given by $\boldsymbol{v}_A = [v_1, v_2, v_3]^T$ and the output vector can be described by the centroid velocity P and the angular velocity of the mobile platform, $\boldsymbol{v} = [v_x, v_y, \omega_z]^T$. Using the vector loop technique and then, applying the differential with respect to time, the relationship between the variables which describe the angular and linear velocity of the mobile platform and the velocities of the links of the planar platform is found. With this relation, the inverse Jacobian of the manipulator is obtained, as shown in Eq. 2 (Albuquerque, A.N., *et al.*, 2016).

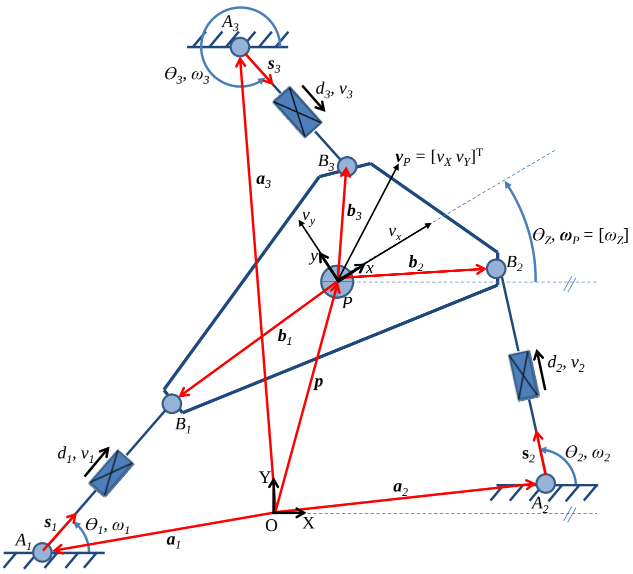

Figure 2. Planar platform with three degrees of freedom.

$$\dot{\mathbf{q}} = \begin{bmatrix} v_1 \\ v_2 \\ v_3 \end{bmatrix} = \mathbf{J}^{-1}\dot{\mathbf{x}} = \begin{bmatrix} \cos\theta_1 & \sin\theta_1 & b_{1X}\sin\theta_1 - b_{1Y}\cos\theta_1 \\ \cos\theta_2 & \sin\theta_2 & b_{2X}\sin\theta_2 - b_{2Y}\cos\theta_2 \\ \cos\theta_3 & \sin\theta_3 & b_{3X}\sin\theta_3 - b_{3Y}\cos\theta_3 \end{bmatrix} \begin{bmatrix} \dot{X} \\ \dot{Y} \\ \dot{\theta} \end{bmatrix} \tag{2}$$

in which θ_i are given by Eq. 3 (with i = 1, 2 and 3). Rewriting Eq. 2 in function of $tan(\theta_i)$, differentiating both sides, and manipulating the terms in order to put in evidence the absolute linear velocities and angular velocity of the platform, we obtain the inverse Jacobian that relates these velocities to the angular velocity of each of the members (Eq. 4).

$$\theta_i = tan^{-1}\left(\frac{b_{iY} - a_{iY}}{b_{iX} - a_{iX}}\right) = tan^{-1}\left(\frac{Y + b_{ix}\sin\theta + b_{iy}\cos\theta - a_{iY}}{X + b_{ix}\cos\theta - b_{iy}\sin\theta - a_{iX}}\right) \tag{3}$$

$$\boldsymbol{\omega}_A = \begin{bmatrix} \omega_1 \\ \omega_2 \\ \omega_3 \end{bmatrix} = \mathbf{J}_\theta^{-1} \begin{bmatrix} v_X \\ v_Y \\ \omega_Z \end{bmatrix} = \begin{bmatrix} \frac{(a_{1Y}-b_{1Y})cos^2(\theta_1)}{(b_{1X}-a_{1X})^2} & \frac{cos^2(\theta_1)}{(b_{1X}-a_{1X})} & \frac{cos^2(\theta_1)}{(b_{1X}-a_{1X})^2} j_{\theta 1} \\ \frac{(a_{2Y}-b_{2Y})cos^2(\theta_2)}{(b_{2X}-a_{2X})^2} & \frac{cos^2(\theta_2)}{(b_{2X}-a_{2X})} & \frac{cos^2(\theta_2)}{(b_{2X}-a_{2X})^2} j_{\theta 2} \\ \frac{(a_{3Y}-b_{3Y})cos^2(\theta_3)}{(b_{3X}-a_{3X})^2} & \frac{cos^2(\theta_3)}{(b_{3X}-a_{3X})} & \frac{cos^2(\theta_3)}{(b_{3X}-a_{3X})^2} j_{\theta 3} \end{bmatrix} \begin{bmatrix} \dot{X} \\ \dot{Y} \\ \dot{\theta} \end{bmatrix} \tag{4}$$

$j_{\theta i}$ is given by Eq. 5, with i = 1, 2, 3, $c\theta = cos(\theta)$ and $s\theta = sin(\theta)$.

$$j_{\theta i} = \left(b_{ix}\, c\,\theta \text{ - } b_{iy}\, s\,\theta\right)\left(b_{iX}\text{-}a_{iX}\right)+\left(b_{ix}\, s\,\theta + b_{iy}\, c\,\theta\right)\left(b_{iY}\text{-}a_{iY}\right) \tag{5}$$

In a graph that correctly describes the kinematics (1 and 0 junctions, transformers and gyrators), the dynamics (capacitors, inertias and resistors) can be imposed without the risk of creating models where the main constraints of mechanical systems are violated: geometric or kinematic ties (Karnopp, D.C., *et al.*, 1990). In this model, speed conditions are imposed by ideal velocity sources, that is, a source of velocity for v_X, v_Y and ω_Z. Besides these velocities, the others 1 junctions (of common velocities) indicates the linear (v_1, v_2 e v_3) and angular velocities (ω_1, ω_2 e ω_3) of the actuators. Thus, the inverse kinematics of the planar platform via multibond graphs is represented as shown in Fig. 3, whereby the modulated transformer type represents the matrices $\mathbf{J}^{-1}$ (Eq. 2) and $\mathbf{J}_\theta^{-1}$ (Eq. 4).

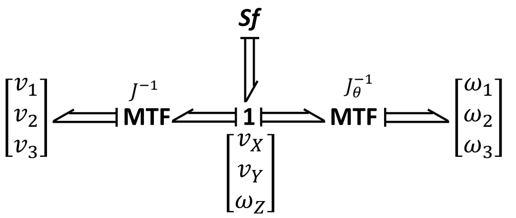

Figure 3. Multibond graphs representation of the planar platform inverse kinematics.

2.2 Direct dynamic model

According to (Karnopp, D.C., *et al.*, 1990), when possible, both completely match the power variables on the inputs and outputs of the subsystems (same type and direction of power flow) and a consistent cause and effect relation (which variables enter and which come out the models to be coupled), the resulting model is fully equivalent to that which would be obtained analytically, allowing your simulation from the simple connection of the modules. Considering the inertia effects of the moving platform, with mass m_P and mass moment of inertia J_{Pzz}, the multibond graphs structure of the direct dynamics model of the planar platform with three degrees of freedom is shown in Fig. 4. Using the concepts, elements and the graphical representation of the Bond Graph Technique, was further added the inertial effects of the bodies that compound the actuators, introducing the terms m_{Ai} and J_{Ai}, which correspond to the mass and moments of inertia of the actuators, with i = 1, 2 and 3. It was also included in this model the equivalent viscous friction in the rotation joints (Albuquerque, A.N., *et al.*, 2017).

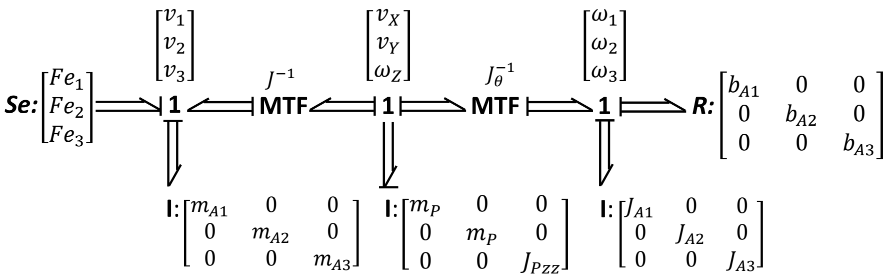

Figure 4. Multibond graphs representation of the planar platform dynamics.

From the model in the Fig. 5, the constitutive equations of the inertia elements (I) with integral (or natural) causality are written in their differential form. Thus, making explicit the efforts, inserting this equation into the junction structures equations and replacing the constitutive equations of the inertial elements with differential (forced) causality, the resistors elements (R) and the modulated transformers (MTF), the Eq. 6 is obtained.

$$\mathbf{M}_P\dot{\mathbf{v}}=\mathbf{J}^{-T}\mathbf{f}_e-\mathbf{J}^{-T}\mathbf{M}_A\dot{\mathbf{v}}_A-\mathbf{J}_\theta^{-T}\mathbf{J}_A\dot{\boldsymbol{\omega}}_A-\mathbf{J}_\theta^{-T}\mathbf{B}_A\boldsymbol{\omega}_A \tag{6}$$

Substituting the equations from the derivatives of the Jacobian matrices and the Eq. 4 into the Eq. 6 and solving the algebraic loops associated to the storage elements with differential causality, the state-space equations are obtained (Eq. 7), with $\mathbf{M}_1$ and $\mathbf{M}_2$ given by Eq. 8 and 9, respectively.

$$\dot{\mathbf{v}}=\left(\mathbf{M}_1^{-1}\mathbf{M}_2\right)\mathbf{v}+\left(\mathbf{M}_1^{-1}\mathbf{J}^{-T}\right)\mathbf{f}_e \tag{7}$$

$$\mathbf{M}_1=\mathbf{M}_P+\mathbf{J}^{-T}\mathbf{M}_A\mathbf{J}^{-1}+\mathbf{J}_\theta^{-T}\mathbf{J}_A\mathbf{J}_\theta^{-1} \tag{8}$$

$$\mathbf{M}_2=-\mathbf{J}^{-T}\mathbf{M}_A\dot{\mathbf{J}}^{-1}-\mathbf{J}_\theta^{-T}\mathbf{J}_A\dot{\mathbf{J}}_\theta^{-1}-\mathbf{J}_\theta^{-T}\mathbf{B}_A\mathbf{J}_\theta^{-1} \tag{9}$$

2.3 Dynamic model of the actuation system

The property of modularity, one of the major advantages of the technique, enables the development of complex systems models from simple subsystems (or modules), since these are created predicting the manner in which they will engage each other. This can be done by passive (open) connections or active connections. In the case of the actuation elements (with two or more ports), it is mandatory the use of passive connections, because there is power interaction effectively, resulting in the loading effect, represented in the bond graphs by the causal bar (Speranza Neto *et al*., 2005).

Figure 5 presents the electric actuator scheme used in this modeling. An electric motor provides power to the actuation system through a torque T_m and an angular velocity ω_m. This power is then transmitted to a leadscrew by a gear set. In bond graphs modeling, motors can, in general, be considered, as effort sources.

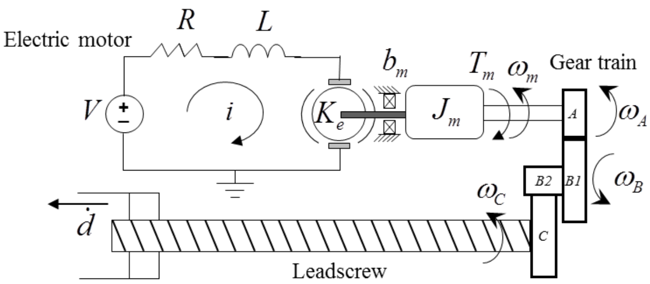

Figure 5. Electric actuator scheme.

In the dynamic model of the actuation system were considered the inertia of the motor (J_m), of the gear train (J_C), of the actuator rod (m_A) and also the viscous friction coefficients b_m, b_C and b_A associated with these elements. Figure 6 presents the bond graph structure of the actuation system, where n_e is the transmission ratio between the gears A and C. The leadscrew D has the same velocity of C, ω_C. Through the leadscrew nut, which is coupled to the actuator rod, this movement becomes linear with velocity $\dot{d}$. This relation is given by $n_P = 0{,}5.\pi^{-1}.p.Ne$, where p is the leadscrew pitch and Ne refers to type of thread. In the electrical circuit model, R, L and K_e are the resistance, the inductance and the electromagnet constant of the motor, respectively.

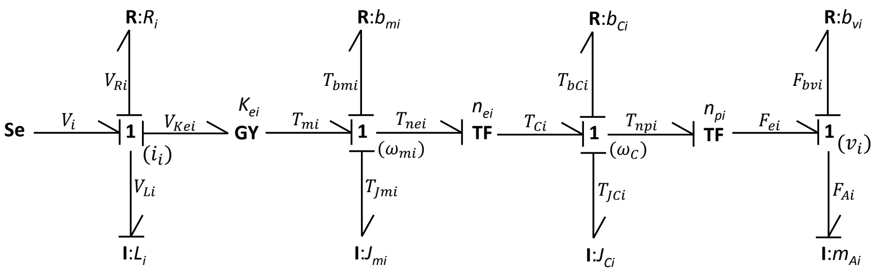

Figure 6. Bond graphs for the electric linear actuator.

Using the Bond Graph Technique formulation, Eq. 10 and 11 are obtained. Eq. 10 describes the electric DC motor with inputs V_i and i_i and output ω_{mi} (left part of the bond graph in Fig. 14). Equation 11 describes the mechanical transmission and the load effect on the actuator. The elimination of the electric dynamics, which has time constants of smaller orders of magnitude than the mechanical dynamics, is made by considering the values of L_i approximately equal to zero (for i = 1, 2 and 3). With this, Eq. 12 is obtained and, substituting that in Eq. 11, the state-space equation (Eq. 13) is obtained.

$$L_i \frac{di_i}{dt} = V_i - R_i i_i - K_{ei}\omega_{mi} \tag{10}$$

$$\left(m_{Ai}{n_{pi}}^2{n_{ei}}^2 + J_{mi} + J_{Ci}{n_{ei}}^2\right)\frac{dv_i}{dt} = K_{ei}n_{pi}n_{ei}i_i - \left(b_{Ci}{n_{ei}}^2 + b_{mi} + b_{vi}{n_{pi}}^2{n_{ei}}^2\right)v_i \tag{11}$$

$$i_i = \frac{V_i}{R_i} - \frac{K_{ei}\omega_{mi}}{R_i} = \frac{V_i}{R_i} - \frac{K_{ei}v_i}{R_i n_{pi} n_{ei}} \tag{12}$$

$$\left(m_{Ai}{n_{pi}}^2{n_{ei}}^2 + J_{mi} + J_{Ci}{n_{ei}}^2\right)\frac{dv_i}{dt} = \frac{K_{ei}n_{pi}n_{ei}V_i}{R_i} - \left(b_{Ci}{n_{ei}}^2 + b_{mi} + b_{vi}{n_{pi}}^2{n_{ei}}^2 + \frac{{K_{ei}}^2}{R_i}\right)v_i \tag{13}$$

2.4 Dynamic model of the coupled system

Figure 7 shows the coupled dynamic model represented using multiband graphs. The actuators models are coupled to the planar platform model through the 1 junctions that represents the actuator output speed, v_i, with i = 1, 2 and 3. Using the Bond Graph Technique formulation, the state-space equation, where $\boldsymbol{v}$ is the state vector and $\boldsymbol{s}_e$ is the input vector (Eq. 16) is obtained, with $\mathbf{M}_3$ and $\mathbf{M}_4$ given by Eq. 14 and 15, respectively.

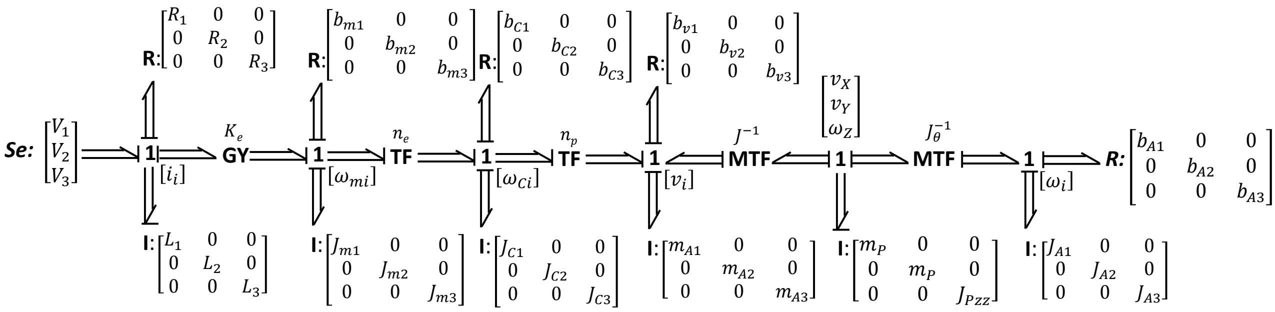

Figure 7. Complete bond graph representation for the 3-R<u>P</u>R parallel mechanism.

$$\mathbf{M}_3 = \mathbf{M}_\mathrm{P} + \mathbf{J}^{-\mathrm{T}}\mathbf{M}_{\mathrm{Aa}}\mathbf{J}^{-1} + \mathbf{J}_\theta^{-\mathrm{T}}\mathbf{J}_\mathrm{A}\mathbf{J}_\theta^{-1} \tag{14}$$

$$\mathbf{M}_4 = -\mathbf{J}^{-\mathrm{T}}\mathbf{B}_{\mathrm{Av}}\mathbf{J}^{-1} - \mathbf{J}^{-\mathrm{T}}\mathbf{M}_{\mathrm{Aa}}\dot{\mathbf{J}}^{-1} - \mathbf{J}_\theta^{-\mathrm{T}}\mathbf{J}_\mathrm{A}\dot{\mathbf{J}}_\theta^{-1} - \mathbf{J}_\theta^{-\mathrm{T}}\mathbf{B}_\mathrm{A}\mathbf{J}_\theta^{-1} \tag{15}$$

$$\dot{\mathbf{v}} = \left({\mathbf{M}_3}^{-1}\mathbf{M}_4\right)\mathbf{v} + \left({\mathbf{M}_3}^{-1}\mathbf{J}^{-\mathrm{T}}\right)\mathbf{s}_\mathrm{e} \tag{16}$$

3. SIMULATION AND EXPERIMENTAL RESULTS

3.1 Inverse kinematics simulation

A set of simulations were made to validate the inverse geometric model (vector loop equation) and the inverse kinematic model (using the matrices $\mathbf{J}^{-1}$ and $\mathbf{J}_\theta^{-1}$). Table 1 presents the geometric parameters of the mechanism.

Table 1. Geometric parameters.

Identification	Symbol	Value
A_1 joint coordinates in reference frame A (mm)	$\boldsymbol{a}_1$	[-389.14 -224.67]
A_2 joint coordinates in reference frame A (mm)	$\boldsymbol{a}_2$	[389.14 -224.67]
A_3 joint coordinates in reference frame A (mm)	$\boldsymbol{a}_3$	[0.00 449.34]
B_1 joint coordinates in reference frame B (mm)	$\boldsymbol{b}_1$	[-125.00 -72.17]
B_2 joint coordinates in reference frame B (mm)	$\boldsymbol{b}_2$	[125.00 -72.17]
B_3 joint coordinates in reference frame B (mm)	$\boldsymbol{b}_3$	[0.00 144.34]
Linear actuator fixed length (mm)	L_{min}	255.00
Stroke of the linear actuator (mm)	S	100.00

Using the Jacobian matrices from the Eq. 2 and 4, the time response of the limbs was obtained for the input functions shown in Eq. 17. Figures 8.a and 8.b shows the linear displacements and velocities of the actuators, respectively.

$$\begin{cases} \dot{X} = 50.00 sin(\pi t) \text{ mm/s} \\ \dot{Y} = 50.00 sin(\pi t) \text{ mm/s} \\ \dot{\theta} = 0.785 sin(\pi t) \text{ rad/s} \end{cases} \tag{17}$$

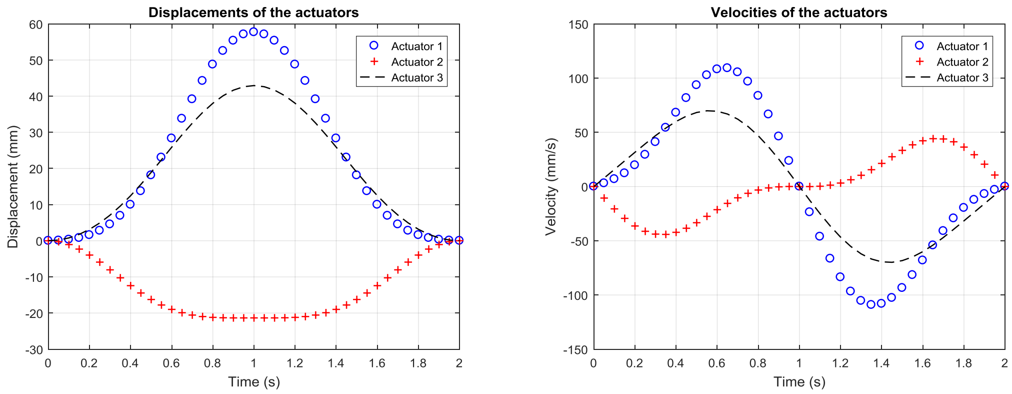

(a) (b)

Figure 8. Linear and angular displacements and velocities of the actuators.

3.2 Direct dynamics simulation

In the simulation of the dynamic model were considered the mass and the mass moment of inertia of the moving platform, m_P and J_{Pzz}, the mass and the mass moment of inertia of the actuators, m_{A1}, m_{A2}, m_{A3} and J_{A1}, J_{A2}, J_{A3}, and the viscous friction coefficients from the actuators joints, b_{A1}, b_{A2} and b_{A3}. Table 2 presents the parameters used in this simulation. The time response of the limbs was obtained for the inputs shown in Fig. 9.a. Two pulses with amplitudes 5 N and –5 N, widths of 0.1 s and interval of 0.1 s between them were given by the actuator 1. Figures 9.b shows the linear accelerations and Fig. 9.c shows the linear velocities of the moving platform.

Table 2. Planar mechanism simulation parameters.

Identification	**Symbol**	**Value**
Mass of the platform (kg)	m_P	0.578
Mass moment of inertia of the platform (kg.m^2)	J_{Pzz}	4.50x10^{-3}
Mass of the actuator rod (kg)	m_{A1}, m_{A2}, m_{A3}	0.175
Mass moment of inertia of the actuator (kg.m^2)	J_{A1}, J_{A2}, J_{A3}	7.28x10^{-3}
Viscous friction coefficient of the joints (N.s.m^{-1})	b_{A1}, b_{A2}, b_{A3}	0.006

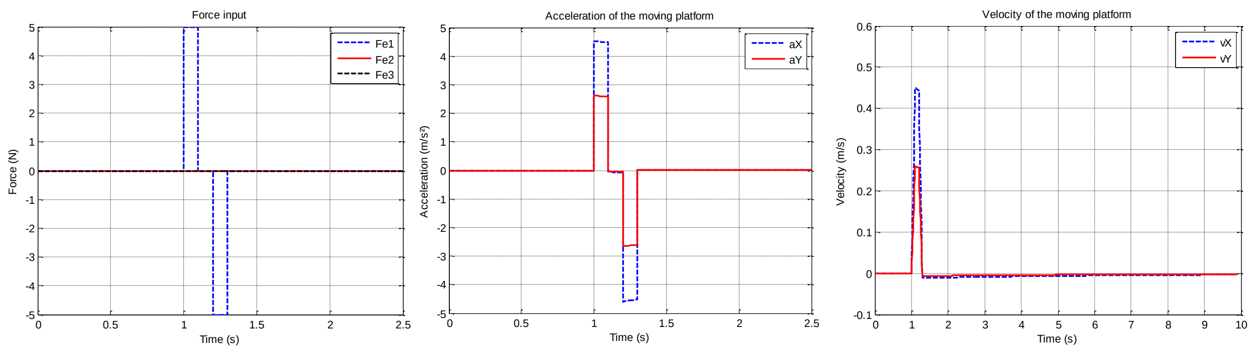

(a) (b) (c)

Figure 9. Forces given by the actuators (a); linear and angular accelerations (b) and velocities (c) of the moving platform.

3.3 Actuating system characterization

The actuator system model parameters were obtained by a set of experiments using a small scale electric motors dynamometer. Figure 10.a shows the characteristic curve for a given duty cycle ratio and Fig. 10.b. shows the motor behavior curves used in the mechanism control system.

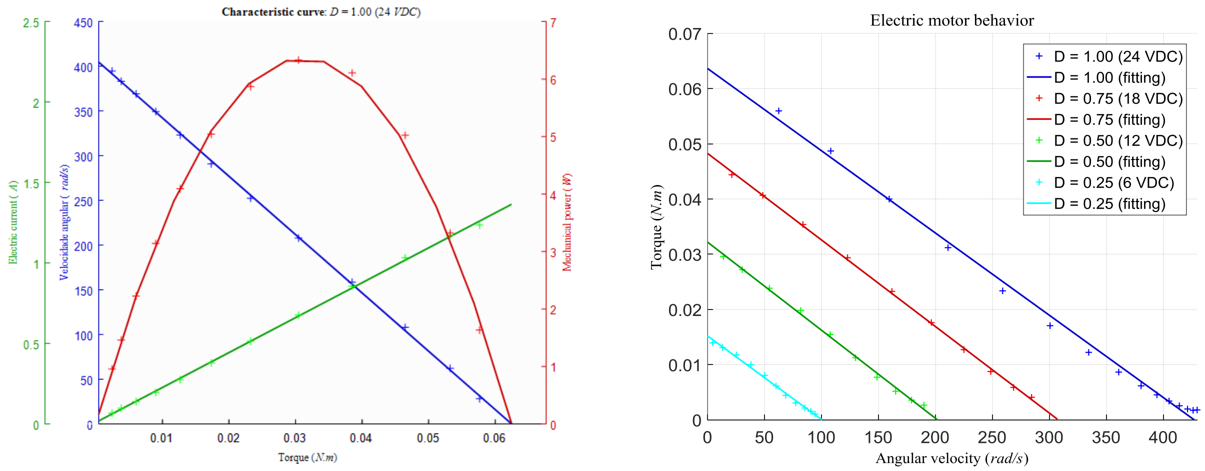

(a) (b)

Figure 10. Characteristic curve for duty cycle = 100 % (a) and motor behavior curves (b).

3.4 Coupled model simulation

Figure 12 shows the time response of the actuators for different values of proportional gain for a given input ([X = 0.0 mm, Y = 20.0 mm, θ = 0.00 rad]) using the control strategy shown in Fig. 11, where G^{-1} represents the inverse geometric model an J^{-1} represents the inverse Jacobian model of the mechanism. The reference values for the steady state are [d_1 = 10.5 mm, d_2 = 10.5 mm, d_3 = -20,0 mm].

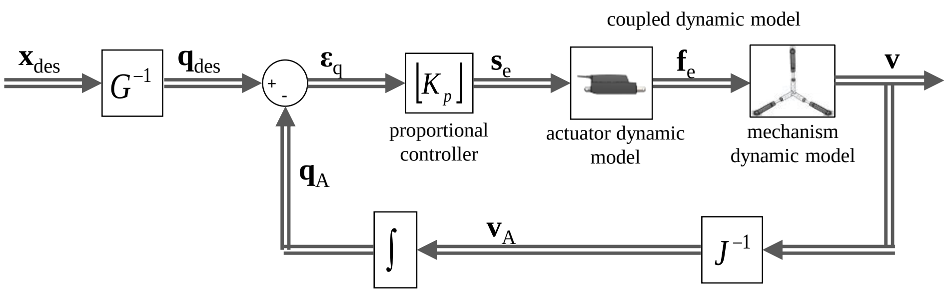

Figure 11. Position control strategy.

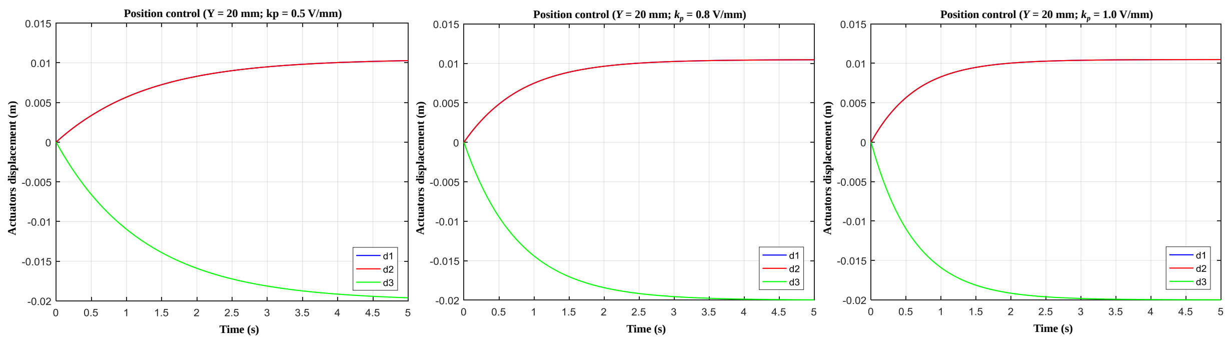

(a) (b) (c)

Figure 12. Time response for $Y(t)$ = 20 mm. (a) k_p = 0.5; (b) k_p = 0.8; (c) k_p = 1.0.

3.5 Experimental results

The models were validated by a set of experiments using the platform shown in Fig. 1. For example, Fig. 13 shows the time response of the actuator 3 for different values of proportional gain for a given input ([X = 0.0 mm, Y = 20.0 mm, θ = 0.00 rad]).

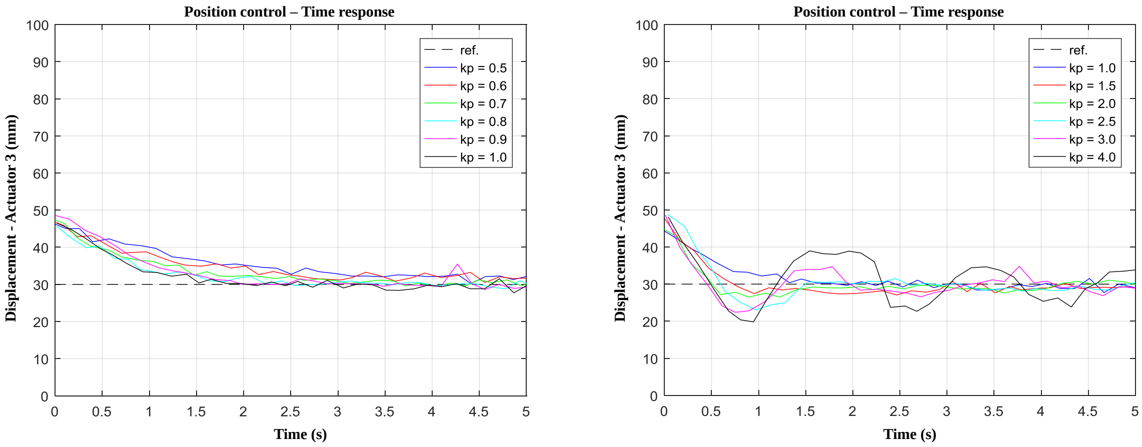

(a) (b)

Figure 13. Time response for different values of gain. (a) k_p from 0.5 to 1.0; (b) k_p from 1.0 to 4.0.

4. CONCLUSIONS

In this work the analytical form of the dynamic model of a 3-RPR parallel mechanism through the characterization of the power flow between its components was presented. From the geometrical relations associated to the displacement of their degrees of freedom, the kinematic relations associated to their velocities were determined. Considering the power flow between the degrees of freedom and between these and the actuating elements, the equilibrium relations of the forces and torques were obtained. This approach adopted the same fundamentals, concepts and elements of the Bond Graph Technique.

A set of simulations were performed to evaluate this approach, using the real data (geometry, inertia, damping, actuators forces, etc) from a planar mechanism designed and built especially for the purpose to compare the simulated and experimental results. This comparison validates the dynamic model. The ongoing work focuses in implement a IMU based control strategy in the built platform (Fig. 14).

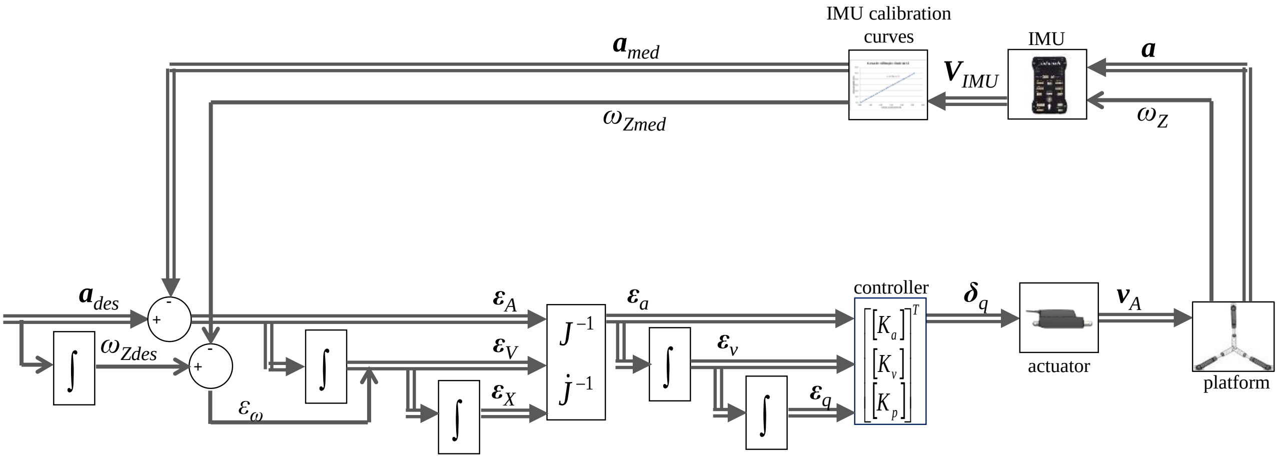

Figure 14. IMU based control strategy

5. ACKNOWLEDGEMENTS

The authors of this work would like to thank FAPERJ and CNPq for the financial support.

6. REFERENCES

Albuquerque, A.N., 2017. “Dinâmica e controle de mecanismos: integração modelo analítico fechado, transdutores inerciais e atuadores elétricos lineares”. *Doctoral dissertation (in portuguese), Pontifical Catholic University, Department of Mechanical Engineering*. Rio de Janeiro, Brazil.

Albuquerque, A.N., Speranza Neto, M. and Meggiolaro, M.A., 2017. “Dynamic modeling and simulation of a parallel planar mechanism using bond graph (power flow) approach”. In *Proceedings of the XVII International Symposium on Dynamic Problems of Mechanics - DINAME 2017*. São Sebastião, SP, Brazil.

Albuquerque, A.N., Speranza Neto, M. and Meggiolaro, M.A., 2016. “Dynamic models of parallel mechanisms using power flow approach”. In *IX Congresso Nacional de Engenharia Mecânica - CONEM 2016*. Fortaleza, Brazil.

Bennett, D.J. and Hollerbach, J.M., 1991. “Autonomous calibration of single-loop closed kinematic chains formed by manipulators with passive endpoint constraints”. *IEEE Transactions on Robotics and Automation*, Vol. 7, n° 5.

Chironis N., 1991. “Mechanisms and Mechanical Devices”. *Sourcebook, McGraw-Hill*.

Costa Neto, R.T., 2008. “Modelagem e integração dos mecanismos de suspensão e direção de veículos terrestres através do fluxo de potência”. *Doctoral dissertation (in portuguese), Pontifical Catholic University, Department of Mechanical Engineering*. Rio de Janeiro, Brazil.

Fischer, I.S. and Chu, T., 2001. “Numerical analysis of the displacement in multi-loop mechanisms”. *Mechanics Research Communication, vol. 28, n° 2*. USA.

Golin, J.F., Martins, D. and Pieri, E.R., 2011. “Modelagem de um manipulador paralelo em contato com um meio rígido através de grafos e helicoides”. *In 10th Brazilian Conference on Dynamics, Control and Their Applications - DINCON 2011*. Águas de Lindoia, Brazil.

Karnopp, D.C., Margolis, D.L. and Rosenberg, R.C., 1990. “System dynamics: A unified approach”. *2nd Edition, John Wiley & Sons*.

Karnopp, D.C. and Rosenberg, R.C., 1968. “Analysis and simulation of multiport systems. The bond graph approach to physical system dynamics”. *The M.I.T. Press*.

Khandelwal, S. and Chevallereau, C., 2013. “Estimate of the trunk attitude of a humanoid by data fusion of inertial sensors and joint encoders”. In *Proceedings of the Sixteenth International Conference on Climbing and Walking Robots*. Sydney, Australia.

Kim, J., Kim, K. and Lee, J.Y., 2001. “Solving 3D geometric constraints for closed-loop assemblies”. In *The 5th International Conference on Engineering Design & Automation*. Las Vegas, USA.

Mohamed, M.G. and Gosselin, C.M., 2005. “Design and analysis of kinematically redundant parallel manipulators with configurable platforms”. *IEEE Transactions on Robotics, vol. 21, n° 3*. USA.

Rosenberg, R.C. and Karnopp, D.C., 1983. “Introduction to physical system dynamics”. *McGraw-Hill*.

Speranza Neto, M., 1999. “Procedimento para acoplamento de modelos dinâmicos através do fluxo de potência”. In *XV Brazilian Congress of Mechanical Engineering – COBEM 99 (in portuguese)*. São Paulo, Brazil.

Speranza Neto, M., 2007. “Dinâmica de um corpo rígido através do fluxo de potência”. *Lecture notes (in portuguese), Pontifical Catholic University, Department of Mechanical Engineering*. Rio de Janeiro, Brazil.

Speranza Neto, M. and Silva, F.R., 2005. “Modelagem e análise de sistemas dinâmicos”. *Lecture notes (in portuguese), Pontifical Catholic University, Department of Mechanical Engineering*. Rio de Janeiro, Brazil.

Tsai, L.W., 1999. “Robot analysis – The mechanical of serial and parallel manipulators”. *Department of Mechanical Engineering and Institute for Systems Research, University of Maryland. John Wiley and Sons, Inc*. USA.

Yildiz, I., Ömürlü, V.E. and Sagirli, A., 2008. “Dynamic modeling of a generalized Stewart platform by bond graph method utilizing a novel spatial visualization technique”. *International Review of Mechanical Engineering*. Turkey.

Wang, Y., 2008. “Symbolic kinematics and dynamics analysis and control of a general Stewart parallel manipulator”. *Master’s thesis, State University of New York at Buffalo, Department of Mechanical and Aerospace Engineering*. Buffalo, USA.

Zhao, Q. and Gao, F., 2012. “Bond graph modelling of hydraulic six-degree-of-freedom motion simulator”. In *Proceedings of the Institution of Mechanical Engineers, Part C: Journal of Mechanical Engineering Science*. USA.

7. RESPONSIBILITY NOTICE

The authors are the only responsible for the printed material included in this paper.